Spatially Structured Optical Effects in a Four-Level Quantum System Near a Plasmonic Nanostructure

Hamid R. Hamedi,* Vassilios Yannopapas, and Emmanuel Paspalakis

The light–matter interaction for a four-level double-V-type quantum system interacting with a pair of weak probe fields while located near a 2D array of metal-coated dielectric nanospheres is studied. A situation is considered in which one of the probe field carries an optical vortex, that is, an electromagnetic field with optical angular momentum, and the other probe field has no vortex. It is demonstrated that due to the phase sensitivity of the closed-loop double V-type quantum system, the linear and nonlinear susceptibility of the non-vortex probe beam depends on the azimuthal angle and orbital angular momentum (OAM) of the vortex probe beam. This feature is missing in an open four-level double V-type quantum system interacting with free-space vacuum, as no quantum interference occurs in this case. The azimuthal dependence of optical susceptibility of the quantum system is used to determine the regions of spatially structured transparency.

1. Introduction

Growing attention has recently emerged in the generation of twisted light beams due to their potential application in quantum information processing,[1,2] optical micromanipulation,[3] biosciences, [4] and microtrapping and alignment.[5] Such beams of light (the so-called optical vortices) carry orbital angular momentum (OAM) with helical wavefronts focusing to rings, rather than points. The interaction of such structured light beams with cold atoms results in a plethora of interesting effects, including light-induced-torque,[6] atom vortex beams,[7] entanglement of OAM states of photon pairs,[8] OAM-based four-wave mixing,[9,10] spatially dependent electromagnetically induced transparency (EIT)

Dr. H. R. Hamedi
Institute of Theoretical Physics and Astronomy
Vilnius University
Saulėtekio 3, Vilnius LT-10257, Lithuania
E-mail: hamid.hamedi@tfai.vu.lt
Prof. V. Yannopapas
School of Applied Mathematics and Physics
Department of Physics
National Technical University of Athens
Athens 15780, Greece
Prof. E. Paspalakis
Materials Science Department
School of Natural Sciences
University of Patras
Patras 26504, Greece

and its applications,[11–17] as well as vortex slow light and transfer of optical vortices between light fields.[18–29]

Another area of research in photonics that has attracted significant attention in current years studies the modification of the optical properties of quantum systems that are placed near metallic or metal-dielectric (plasmonic) nanostructures. The coherent interaction of light with the quantum systems near plasmonic nanostructures may lead to several quantum coherence and interference phenomena with updated properties compared to the isolated quantum systems. Some of these effects are optical transparency and slow light,[30–32] gain without inversion,[33–36] control of spontaneous emission,[37–41] Fano effects in energy absorption,[42–44] controlled quantum entanglement,[45,46] electromagnetically induced grating,[47–50] existence and manipulation of optical bistability,[51,52] enhanced second-harmonic generation,[53] modified four-wave mixing,[54,55] and enhanced Kerr nonlinearity.[56–63]

An interesting topic is the interplay of quantum systems near plasmonic nanostructures and optical vortices. The usage of the optical vortex beam together with a plasmonic nanostructure may result in a significant modification of optical response for the quantum system when compared to the case where the quantum system is just in free space. To the best of our knowledge, a similar analysis on interaction of quantum systems near plasmonic nanostructures with structured light has not been reported. Here, we present a study in this area. Specifically, we study the interaction of a four-level, double-V-type quantum system with two electromagnetic fields, an electromagnetic field with OAM, and another regular field (without OAM), when the quantum system is located near a 2D array of metal-coated dielectric nanospheres. The double-V-type quantum system displays effects of quantum interference in spontaneous emission when placed near the periodic plasmonic nanostructure[38] and its optical properties have been analyzed in various studies exhibiting very interesting effects.[30,31,36,41,46–48,50,56,63] In this work, we study the angular dependence of optical susceptibility of the quantum system. We show that the azimuthally varying linear and nonlinear patterns can be controlled though different external parameters such as the distance of the quantum system from the surface of plasmonic nanostructure and the vorticity of twisted probe beam. We also demonstrate that such a scheme can be used to distinguish the OAM state of a weak vortex beam by mapping the absorption of nonvortex probe field in the transverse spatial profile.
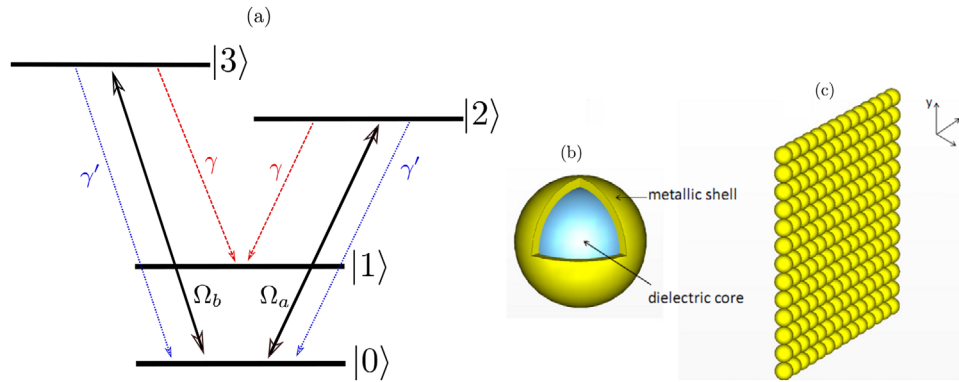
Figure 1. Schematic diagram of the four-level double-V-type quantum system (a). A metal-coated dielectric nanosphere (b) and a 2D array of such spheres (c).

The paper is organized as follows: In Section 2 we present the basic equations, based on the density matrix formulation, where the decay rates entering in the density matrix equations are calculated by electromagnetic calculations and are modified by the presence of the plasmonic nanostructure. We also use the density matrix equations and calculate the linear and the third-order susceptibility of the non-vortex field in the presence of the vortex field. Then, we use the derived susceptibilities in Section 3 to study the azimuthally varying linear and nonlinear patterns and present their control. Finally, in Section 4 we conclude our findings.

2. Theoretical Model and Formulation

In this section, we present in detail the theory of the light–matter interaction of the four-level quantum system near the plasmonic nanostructure. The theory has been presented earlier in other works, for example, ref. [63], but for completeness of the present work and for giving the opportunity to the interested reader to repeat the calculations, we also present it here.

We consider a four-level quantum system involving two closely lying upper states $|2\rangle$ and $|3\rangle$, and two lower states $|0\rangle$ and $|1\rangle$, building a double-V level configuration (**Figure 1**a). Such a quantum system is placed in vacuum at distance d from the surface of the plasmonic nanostructure. It is located right opposite the center of a nanosphere, that is, at the center of the 2D unit cell of the periodic plasmonic nanostructure. The resulting quantum interference p can be maximized at this lateral placement of the quantum system. The upper states $|2\rangle$ and $|3\rangle$ indicate two Zeeman sublevels ($J = 1$, $M_J = \pm 1$), while the two lower states $|0\rangle$ and $|1\rangle$ are corresponding levels with $J = 0$. The dipole moment operator is defined by

$$\vec{\mu} = \mu'(|2\rangle\langle 0|\hat{\varepsilon}_- + |3\rangle\langle 0|\hat{\varepsilon}_+) + \mu(|2\rangle\langle 1|\hat{\varepsilon}_- + |3\rangle\langle 1|\hat{\varepsilon}_+) + H.c., \quad (1)$$

where $\hat{\varepsilon}_\pm = (\mathbf{e}_z + i\mathbf{e}_x)/\sqrt{2}$ show the right-rotating ($\hat{\varepsilon}_+$) and left-rotating ($\hat{\varepsilon}_-$) unit vectors, whereas μ and μ' are real.

We consider the case that the quantum system interacts with two circularly polarized continuous-wave electromagnetic laser fields with total electric field

$$\vec{E}(t) = \hat{\varepsilon}_+ E_a \cos(\omega_a t + \phi_a) + \hat{\varepsilon}_- E_b \cos(\omega_b t + \phi_b) \quad (2)$$

where $E_a(E_b)$, $\omega_a(\omega_b)$, and $\phi_a(\phi_b)$ characterize the electric-field amplitude, the angular frequency, and the individual phase for the field $a(b)$, respectively. The first laser field a couples the lower level $|0\rangle$ and the upper state $|2\rangle$, while the second laser field b acts between the lower level $|0\rangle$ and the upper state $|3\rangle$. The transition $|0\rangle \leftrightarrow |1\rangle$ is dipole forbidden. We also assume both fields with equal frequencies $\omega_a = \omega_b = \omega_L$.

We further assume that the upper V-type subsystem involving $|2\rangle$, $|3\rangle$ and $|1\rangle$ lies within the surface-plasmon bands of the plasmonic nanostructure, while the lower V-type subsystem containing $|2\rangle$, $|3\rangle$ and $|0\rangle$ is spectrally away from the surface-plasmon bands, hence it is not influenced by the plasmonic nanostructure.[30,31,36,38,40,41,46–48,50,56,63] This leads the spontaneous decay in lower V subsystem due to the interaction of the quantum system with the free-space vacuum electromagnetic modes. The quantum configuration considered here can be realized in hyperfine sublevels of D lines in alkali-metal atomic systems, such as ^{85}Rb and ^{87}Rb,[31,32,40] as well as in quantum dots, like in dual CdSe/ZnS/CdSe quantum dots.[31,32]

The Hamiltonian describing the interaction of laser beams and the quantum scheme reads

$$H_e = \hbar\left[\left(-\delta - \frac{\omega_{32}}{2}\right)|2\rangle\langle 2| + \left(-\delta + \frac{\omega_{32}}{2}\right)|3\rangle\langle 3|\right.$$
$$\left. - \left(\frac{\Omega_a e^{i\phi_a}}{2}|0\rangle\langle 2| + \frac{\Omega_b e^{i\phi_b}}{2}|0\rangle\langle 3| + H.c.\right)\right] \quad (3)$$

where $\Omega_a = \mu' E_a/\sqrt{2}\hbar$ and $\Omega_b = \mu' E_b/\sqrt{2}\hbar$ denote the Rabi frequencies for the two fields. Here $\delta = \omega_L - \widetilde{\omega}$ is the detuning from resonance with the average transition energy of states $|2\rangle$ and $|3\rangle$ from state $|0\rangle$ [$\widetilde{\omega} = (\omega_2 + \omega_3)/2 - \omega_0$] and $\omega_{32} = (\omega_3 - \omega_2)/2$, where $\hbar\omega_j = \hbar\omega_j$, $j = 0 - 3$ is the energy of state $|j\rangle$. Note that the transitions $|1\rangle$, $|2\rangle$, $|3\rangle$ are spectrally far from the transitions $|0\rangle$, $|2\rangle$, $|3\rangle$, so they are not driven by the laser fields.

The quantum dynamics of the system is then characterized by the master equation

$$\dot{\rho}_s = -\frac{i}{\hbar}[H_e, \rho_s] + \mathcal{L}\rho_s \quad (4)$$

**ADVANCED
SCIENCE NEWS**

www.advancedsciencenews.com

annalen
der **physik**

www.ann-phys.org

where

$$\mathcal{L}\rho_s = \gamma'(|0\rangle\langle 2|2\rho_s|2\rangle\langle 0| - |2\rangle\langle 2|\rho_s - \rho_s|2\rangle\langle 2|)$$
$$+ \gamma'(|0\rangle\langle 3|2\rho_s|3\rangle\langle 0| - |3\rangle\langle 3|\rho_s - \rho_s|3\rangle\langle 3|)$$
$$+ \gamma(|1\rangle\langle 2|2\rho_s|2\rangle\langle 1| - |2\rangle\langle 2|\rho_s - \rho_s|2\rangle\langle 2|)$$
$$+ \gamma(|1\rangle\langle 3|2\rho_s|3\rangle\langle 1| - |3\rangle\langle 3|\rho_s - \rho_s|3\rangle\langle 3|)$$
$$+ \kappa(|1\rangle\langle 3|2\rho_s|2\rangle\langle 1| - |2\rangle\langle 3|\rho_s - \rho_s|2\rangle\langle 3|)$$
$$+ \kappa(|1\rangle\langle 2|2\rho_s|3\rangle\langle 1| - |3\rangle\langle 2|\rho_s - \rho_s|3\rangle\langle 2|)$$
$$+ \gamma''(|0\rangle\langle 1|2\rho_s|1\rangle\langle 0| - |1\rangle\langle 1|\rho_s - \rho_s|1\rangle\langle 1|) \quad (5)$$

represents the dissipation processes. We assume that the decay rates from the two upper levels to the lower level are the same. The difference in energy of states $|2\rangle$ and $|3\rangle$ is rather small, that is, ω_{32} is only a few Γ_0 (Γ_0 is the decay rate in free space[38]). The term containing γ'' is very small ($\gamma'' \ll \gamma, \gamma'$) as it arises from a dipole forbidden transition, hence we neglect it by taking $\gamma'' = 0$.

Using Equation (4), one arrives at the following equations for the density matrix elements which describe the dynamics of the light–matter coupling

$$\dot{\rho}_{20} = \left(i\delta + i\frac{\omega_{32}}{2} - \gamma - \gamma'\right)\rho_{20} - \kappa\rho_{30} + i\frac{\Omega_a}{2}(\rho_{00} - \rho_{22})$$
$$- i\frac{\Omega_b}{2}e^{-i\phi}\rho_{23} \quad (6)$$

$$\dot{\rho}_{30} = \left(i\delta - i\frac{\omega_{32}}{2} - \gamma - \gamma'\right)\rho_{30} - \kappa\rho_{20} + i\frac{\Omega_b}{2}e^{-i\phi}(\rho_{00} - \rho_{33})$$
$$- i\frac{\Omega_a}{2}\rho_{32} \quad (7)$$

$$\dot{\rho}_{23} = (i\omega_{32} - 2\gamma - 2\gamma')\rho_{23} + i\frac{\Omega_a}{2}\rho_{03} - i\frac{\Omega_b}{2}e^{i\phi} - \kappa(\rho_{22} + \rho_{33}) \quad (8)$$

$$\dot{\rho}_{00} = 2\gamma'(\rho_{22} + \rho_{33}) - i\frac{\Omega_a}{2}(\rho_{02} - \rho_{20}) - i\frac{\Omega_b}{2}(\rho_{03}e^{-i\phi} - \rho_{30}e^{i\phi}) \quad (9)$$

$$\dot{\rho}_{22} = -2(\gamma + \gamma')\rho_{22} + i\frac{\Omega_a}{2}(\rho_{02} - \rho_{20}) - \kappa(\rho_{23} + \rho_{32}) \quad (10)$$

$$\dot{\rho}_{33} = -2(\gamma + \gamma')\rho_{33} + i\frac{\Omega_b}{2}(\rho_{03}e^{-i\phi} - \rho_{20}e^{i\phi}) - \kappa(\rho_{23} + \rho_{32}) \quad (11)$$

with $\rho_{ij} = \rho_{ji}^*$ $\rho_{00} + \rho_{11} + \rho_{22} + \rho_{33} = 1$ which demonstrates the population conservation. We define $\phi = \phi_b - \phi_a$ as the relative phase of the applied fields. The optical coherence corresponding to the probe transition of $|0\rangle \rightarrow |2\rangle$ $(|0\rangle \rightarrow |3\rangle)$ is $\rho_{20}(\rho_{30})$. The optical coherence corresponding to the probe transitions $|0\rangle \rightarrow |2\rangle$ and $|0\rangle \rightarrow |3\rangle$ are ρ_{20} and ρ_{30}, respectively. The probe fields are very weak and can be treated as a perturbation. The parameter κ denotes the coupling coefficient between states $|2\rangle$ and $|3\rangle$ due to spontaneous emission in a modified anisotropic vacuum[64] (anisotropic Purcell effect) which is responsible for the appearance of quantum interference.[65]

The parameters γ and κ are defined as[37,66–70]

$$\gamma = \frac{\mu_0\mu^2\bar{\omega}^2}{2\hbar}\hat{\varepsilon}_-.\,Im\mathbf{G}(\mathbf{r},\mathbf{r};\bar{\omega}).\hat{\varepsilon}_+ \quad (12)$$

$$\kappa = \frac{\mu_0\mu^2\bar{\omega}^2}{2\hbar}\hat{\varepsilon}_+.\,Im\mathbf{G}(\mathbf{r},\mathbf{r};\bar{\omega}).\hat{\varepsilon}_+ \quad (13)$$

where $\mathbf{G}(\mathbf{r},\mathbf{r};\bar{\omega})$ $[\bar{\omega} = (\omega_3 + \omega_2)/2 - \omega_1]$, $\mathbf{r}$ and μ_0 refer to the dyadic electromagnetic Green's tensor, the position of the quantum emitter and the permeability of vacuum, respectively. Using Equations (12) and (13), the values of γ and κ read[37,66–70]

$$\gamma = \frac{\mu_0\mu^2\bar{\omega}^2}{2\hbar}\,Im\left[G_\perp(\mathbf{r},\mathbf{r};\bar{\omega}) + G_\parallel(\mathbf{r},\mathbf{r};\bar{\omega})\right] = \frac{1}{2}(\Gamma_\perp + \Gamma_\parallel) \quad (14)$$

$$\kappa = \frac{\mu_0\mu^2\bar{\omega}^2}{2\hbar}\,Im\left[G_\perp(\mathbf{r},\mathbf{r};\bar{\omega}) - G_\parallel(\mathbf{r},\mathbf{r};\bar{\omega})\right] = \frac{1}{2}(\Gamma_\perp - \Gamma_\parallel) \quad (15)$$

Here, $G_\perp(\mathbf{r},\mathbf{r};\bar{\omega}) = G_{zz}(\mathbf{r},\mathbf{r};\bar{\omega})$ and $G_\parallel(\mathbf{r},\mathbf{r};\bar{\omega}) = G_{xx}(\mathbf{r},\mathbf{r};\bar{\omega})$ are components of the electromagnetic Green's tensor, with the symbol $\perp(\parallel)$ referring to a dipole oriented normal, along the z axis (parallel, along the x axis) to the surface of the nanostructure. We also define the spontaneous emission rates normal and parallel to the surface by $\Gamma_{\perp,\parallel} = \mu_0\mu^2\bar{\omega}^2\,Im[G_{\perp,\parallel}(\mathbf{r},\mathbf{r};\bar{\omega})]/\hbar$. The degree of quantum interference then can be expressed by

$$p = (\Gamma_\perp - \Gamma_\parallel)/(\Gamma_\perp + \Gamma_\parallel) \quad (16)$$

The maximum quantum interference is obtained in spontaneous emission[65] when $p = \pm 1$, which is only achieved by placing the emitter close to a structure that completely quenches either $\Gamma_\perp$ or $\Gamma_\parallel$. On the other hand, when the emitter is placed in vacuum, $\Gamma_\perp = \Gamma_\parallel$, no quantum interference occurs in the system ($\kappa = 0$).

As can be seen in Figure 1b,c, the plasmonic nanostructure considered here is a 2D array of touching metal-coated silica nanospheres. The dielectric function of the shell is provided by a Drude-type electric permittivity

$$\epsilon(\omega) = 1 - \frac{\omega_p^2}{\omega(\omega + i/\tau)} \quad (17)$$

where ω_p shows the bulk plasma frequency and τ is the relaxation time of the conduction-band electrons of the metal. A typical value of the plasma frequency for gold is $\hbar\omega_p = 8.99$ eV, which can also determine the length scale of the system as $c/\omega_p \approx 22$ nm. In the calculations we have taken $\tau^{-1} = 0.05\omega_p$. The dielectric constant of SiO_2 is taken to be $\epsilon = 2.1$. The lattice constant of the square lattice is $a = 2c/\omega_p$ and the sphere radius $S = c/\omega_p$ with core radius $S_c = 0.7c/\omega_p$. The maximization quantum interference rate p can be achieved by using this particular choice of sphere/core radius and lattice constant. The layered multiple scattering method[37,71–73] is used for the calculation of the spontaneous decay rates next to the plasmonic nanostructure. We consider $\bar{\omega} = 0.632\omega_p$, while the distance between the quantum system and the surface of the plasmonic nanostructure, d, is altered. For the results of $\Gamma_\perp$ and $\Gamma_\parallel$ used here, we refer to Figure 3 in ref. [30]. It is observed that $\Gamma_\parallel$ results in significant suppression and its actual value is markedly lower than the free-space decay rate.

**ADVANCED
SCIENCE NEWS**

www.advancedsciencenews.com

annalen
der **physik**

www.ann-phys.org

In addition, the value of $\Gamma_\perp$ reduces with increasing the distance between the quantum system and the plasmonic nanostructure. For distances close to the plasmonic nanostructure, $\Gamma_\perp$ is much larger than the free-space decay rate. The value of $\Gamma_\perp$ becomes larger than the free-space decay rate for distances up to $0.6c/\omega_p$, while for distances between $0.65c/\omega_p$ and c/ω_p the value of $\Gamma_\perp$ is lower than the free-space decay rate. We note that the plasmonic nanostructure influences the linear and nonlinear susceptibilities through the change of the decay rate of the quantum system γ and the coupling coefficient κ. Both of these terms, as can be seen from Equations (12) to (15), depend on $\Gamma_\parallel$ and $\Gamma_\perp$, which are influenced by the presence of the plasmonic nanostructure and therefore, as we already mentioned above, can change with the distance of the quantum system from the plasmonic nanostructure.

In order to derive the linear and nonlinear electric susceptibilities for the laser field Ω_a, we assume that the probe fields are weak enough such that they are treated as perturbation to the system when reaching the steady-state. The method used here is a third order extension of the method presented in ref. [74], while it is similar to that used in refs. [13] and [63]. Under the weak-field approximation, one can apply the perturbation approach to the density-matrix elements

$$\rho_{ij} = \rho_{ij}^{(0)} + \lambda\rho_{ij}^{(1)} + \lambda^2\rho_{ij}^{(2)} + \lambda^{(3)}\rho_{ij}^{(3)} + \cdots \tag{18}$$

where λ represents a continuously varying parameter ranging from zero to unity. Here the $\rho_{ij}^{(n)}$ with $n = 1, 2, 3$ are of the nth order in the probe beams. Since we are working in the weak field limit (e.g., the probe fields are considered to be weak), the zeroth-order solution is $\rho_{00}^{(0)} = 1$, while the other elements $\rho_{ij}^{(0)} = 0$. Substituting Equation (18) into Equations (6)–(11), the equations of motion for the first- and third order density-matrix elements are then simplified to

$$\dot{\rho}_{20}^{(1)} = \left(i\delta + i\frac{\omega_{32}}{2} - \gamma - \gamma'\right)\rho_{20}^{(1)} - \kappa\rho_{30}^{(1)} + i\frac{\Omega_a}{2} \tag{19}$$

$$\dot{\rho}_{30}^{(1)} = \left(i\delta - i\frac{\omega_{32}}{2} - \gamma - \gamma'\right)\rho_{30}^{(1)} - \kappa\rho_{20}^{(1)} + i\frac{\Omega_b}{2}e^{-i\phi} \tag{20}$$

$$\dot{\rho}_{20}^{(3)} = \left(i\delta + i\frac{\omega_{32}}{2} - \gamma - \gamma'\right)\rho_{20}^{(3)} - \kappa\rho_{30}^{(3)} + i\frac{\Omega_a}{2}\left(\rho_{00}^{(2)} - \rho_{22}^{(2)}\right)$$
$$- i\frac{\Omega_b}{2}e^{-i\phi}\rho_{23}^{(2)} \tag{21}$$

$$\dot{\rho}_{30}^{(3)} = \left(i\delta - i\frac{\omega_{32}}{2} - \gamma - \gamma'\right)\rho_{30}^{(3)} - \kappa\rho_{20}^{(3)} + i\frac{\Omega_b}{2}e^{-i\phi}\left(\rho_{00}^{(2)} - \rho_{33}^{(2)}\right)$$
$$- i\frac{\Omega_a}{2}\rho_{32}^{(2)} \tag{22}$$

We look for the steady-state solutions characterized by the time-independent density matrix elements, giving

$$\rho_{20}^{(1)} = i\frac{\Omega_a}{2}S_1 - i\kappa\frac{\Omega_b}{2}e^{-i\phi}S_2 \tag{23}$$

$$\rho_{30}^{(1)} = i\frac{\Omega_b}{2}e^{-i\phi}S_3 - i\kappa\frac{\Omega_a}{2}S_2 \tag{24}$$

$$\rho_{20}^{(3)} = -a_2\kappa - a_1\left(i\delta - i\frac{\omega_{32}}{2} - \gamma - \gamma'\right) \tag{25}$$

$$\rho_{30}^{(3)} = -a_1\kappa - a_2\left(i\delta + i\frac{\omega_{32}}{2} - \gamma - \gamma'\right) \tag{26}$$

where

$$S_1 = \frac{\left(-i\delta + i\frac{\omega_{32}}{2} + \gamma + \gamma'\right)}{\left(-i\delta + i\frac{\omega_{32}}{2} + \gamma + \gamma'\right)\left(-i\delta - i\frac{\omega_{32}}{2} + \gamma + \gamma'\right) - \kappa^2} \tag{27}$$

$$S_2 = \frac{1}{\left(-i\delta + i\frac{\omega_{32}}{2} + \gamma + \gamma'\right)\left(-i\delta - i\frac{\omega_{32}}{2} + \gamma + \gamma'\right) - \kappa^2} \tag{28}$$

$$S_3 = \frac{\left(-i\delta - i\frac{\omega_{32}}{2} + \gamma + \gamma'\right)}{\left(-i\delta + i\frac{\omega_{32}}{2} + \gamma + \gamma'\right)\left(-i\delta - i\frac{\omega_{32}}{2} + \gamma + \gamma'\right) - \kappa^2} \tag{29}$$

$$a_1 = \frac{-i\frac{\Omega_a}{2}\left(\rho_{00}^{(2)} - \rho_{22}^{(2)}\right) - i\frac{\Omega_b}{2}e^{-i\phi}\rho_{23}^{(2)}}{\left(-i\delta + i\frac{\omega_{32}}{2} + \gamma + \gamma'\right)\left(-i\delta - i\frac{\omega_{32}}{2} + \gamma + \gamma'\right) - \kappa^2} \tag{30}$$

$$a_2 = \frac{-i\frac{\Omega_b}{2}e^{-i\phi}\left(\rho_{00}^{(2)} - \rho_{33}^{(2)}\right) - i\frac{\Omega_a}{2}\rho_{32}^{(2)}}{\left(-i\delta + i\frac{\omega_{32}}{2} + \gamma + \gamma'\right)\left(-i\delta - i\frac{\omega_{32}}{2} + \gamma + \gamma'\right) - \kappa^2} \tag{31}$$

Here, the second-order density matrix elements of Equations (25) and (26) featured in Equations (30) and (31) can be solved to obtain the steady-state solutions $\rho_{ij}^{(2)}$. The expressions for the steady-state solutions $\rho_{ij}^{(2)}$ are:

$$\rho_{11}^{(2)} = -\frac{(r+s)}{2\gamma'} \tag{32}$$

$$\rho_{22}^{(2)} = \frac{2\gamma'\kappa r + \kappa\gamma(r+s)}{4\gamma'\kappa(\gamma+\gamma')} \tag{33}$$

$$\rho_{33}^{(2)} = \frac{2\gamma'\kappa s + \kappa\gamma(r+s)}{4\gamma'\kappa(\gamma+\gamma')} \tag{34}$$

$$\rho_{23}^{(2)} = \frac{\kappa(r+s) - 2\gamma't}{2\gamma'(i\omega_{32} - 2\gamma - 2\gamma')} \tag{35}$$

and $\rho_{00}^{(2)} = 0$, where

$$t = \frac{i\Omega_a}{2}\left(-i\frac{\Omega_b}{2}e^{i\phi}S_3^* + i\kappa\frac{\Omega_a}{2}S_2^*\right)$$
$$- i\frac{\Omega_b}{2}e^{i\phi}\left(i\frac{\Omega_a}{2}S_1 - i\kappa\frac{\Omega_b}{2}e^{-i\phi}S_2\right) \tag{36}$$

$$r = \frac{i\Omega_a}{2}\left(\left(-i\frac{\Omega_a}{2}S_1^* + i\kappa\frac{\Omega_b}{2}e^{i\phi}S_2^*\right) - \left(i\frac{\Omega_a}{2}S_1 - i\kappa\frac{\Omega_b}{2}e^{-i\phi}S_2\right)\right) \tag{37}$$

**ADVANCED
SCIENCE NEWS**

www.advancedsciencenews.com

annalen
der **physik**

www.ann-phys.org

$$s = \frac{i\Omega_b}{2} \left(\left(-i\frac{\Omega_b}{2} e^{i\phi} S_3^* + i\kappa \frac{\Omega_a}{2} S_2^* \right) e^{-i\phi} \right.$$
$$\left. - \left(i\frac{\Omega_b}{2} e^{-i\phi} S_3 - i\kappa \frac{\Omega_a}{2} S_2 \right) e^{i\phi} \right) \qquad (38)$$

Decomposing the susceptibility as

$$\chi \approx \chi^{(1)} + 3\chi^{(3)} E_a^2 / 4 \qquad (39)$$

using

$$\chi(\delta) = \frac{\sqrt{2} N \mu'}{\varepsilon_0 E_a} \rho_{20} \qquad (40)$$

and expanding ρ_{20} in perturbation series, the linear susceptibility $\chi^{(1)}$ and the third-order nonlinear susceptibility $\chi^{(3)}$ can be written as

$$\chi^{(1)}(\delta) = \frac{\sqrt{2} N \mu'}{\varepsilon_0 E_a} \rho_{20}^{(1)} = \frac{N \mu'^2}{\varepsilon_0 \hbar} \frac{\rho_{20}^{(1)}}{\Omega_a} \qquad (41)$$

and

$$\chi^{(3)}(\delta) E_a^2 = \frac{4 N \mu'^2}{3 \varepsilon_0 \hbar} \frac{\rho_{20}^{(3)}}{\Omega_a} \qquad (42)$$

Note that ε_0 is the vacuum permittivity and N is the density of the quantum systems. We now replace Equations (27)–(31) into equations (23), (25) and use Equations (32)–(38). This simplifies Equations (41) and (42) to

$$\chi^{(1)}(\delta) = \frac{N \mu'^2}{\varepsilon_0 \hbar} \frac{-i\kappa A + B(\delta - \frac{\omega_{32}}{2} + i\gamma + i\gamma')}{(-i\delta + i\frac{\omega_{32}}{2} + \gamma + \gamma')(-i\delta - i\frac{\omega_{32}}{2} + \gamma + \gamma') - \kappa^2}$$
$$(43)$$

and

$$\chi^{(3)}(\delta) = \frac{2 N \mu'^4}{3 \varepsilon_0 \hbar^3} \frac{-i\kappa C + D(\delta - \frac{\omega_{32}}{2} + i\gamma + i\gamma')}{(-i\delta + i\frac{\omega_{32}}{2} + \gamma + \gamma')(-i\delta - i\frac{\omega_{32}}{2} + \gamma + \gamma') - \kappa^2}$$
$$(44)$$

where we have defined $x = \frac{\Omega_b}{\Omega_a}$. The expressions for the coefficients A, B, C and D are:

$$A = e^{-i\phi} x \qquad (45)$$

$$B = 1 \qquad (46)$$

$$C = \frac{1}{8} \left[-\frac{2\gamma' f_1 + \gamma f_2}{4\gamma'(\gamma + \gamma')} - \frac{\kappa f_3 + 2\gamma' f_4}{2\gamma'(-i\omega_{32} - 2\gamma - 2\gamma')} \right] \qquad (47)$$

$$D = \frac{1}{8} \left[-\frac{2\gamma' f_5 + \gamma f_6}{4\gamma'(\gamma + \gamma')} - \frac{\kappa f_7 + 2\gamma' f_8}{2\gamma'(i\omega_{32} - 2\gamma - 2\gamma')} \right] \qquad (48)$$

with

$$f_1 = -x^3 e^{-i\phi}(S_3 + S_3^*) + x^2 \kappa e^{-2i\phi} S_2^* + \kappa x^2 S_2 \qquad (49)$$

$$f_2 = -x e^{-i\phi}(S_1 + S_1^*) + \kappa x^2 (S_2 + S_2^*) - x^3 e^{-i\phi}(S_3 + S_3^*)$$
$$- \kappa x^2 e^{-2i\phi}(S_2 - S_2^*) \qquad (50)$$

$$f_3 = -(S_1 + S_1^*) + \kappa x e^{-i\phi} S_2 + x\kappa e^{i\phi} S_2^* - x^2 S_3 + x\kappa S_2 e^{i\phi}$$
$$- x^2 e^{i\phi} S_3^* + \kappa x S_2^* e^{-i\phi} \qquad (51)$$

$$f_4 = x e^{-i\phi}(S_3 + S_1^*) - \kappa S_2 - x^2 \kappa S_2^* \qquad (52)$$

$$f_5 = (S_1 + S_1^*) - x\kappa S_2^* - \kappa x S_2 e^{-i\phi} \qquad (53)$$

$$f_6 = (S_1 + S_1^*) - \kappa x(e^{i\phi} S_2^* + S_2 e^{-i\phi} + S_2^* e^{-i\phi} + S_2 e^{i\phi})$$
$$+ x^2(S_3 + S_3^*) \qquad (54)$$

$$f_7 = x e^{-i\phi}(S_1 + S_1^*) - \kappa x^2(S_2 + S_2^*) - \kappa x^2 e^{-2i\phi}(S_2 + S_2^*)$$
$$+ x^3(e^{-i\phi} S_3 + S_3^*) \qquad (55)$$

$$f_8 = -x^2 S_3^* + x\kappa e^{-i\phi} S_2^* - x^2 S_1 + \kappa x^3 S_2 e^{-i\phi} \qquad (56)$$

The real and imaginary parts of $\chi^{(1)}$ represent then the linear dispersion and absorption, respectively. The real and imaginary parts of the third-order susceptibility $\chi^{(3)}$ are related to the Kerr nonlinearity and nonlinear absorption, respectively. Setting $\omega_{32} = 0$ and $\delta = 0$, Equations (43) and (44) simplify, their real and imaginary parts can be expressed as

$$Im(\chi^{(1)}(\delta = 0)) = \frac{N \mu'^2}{\varepsilon_0 \hbar} \frac{\gamma + \gamma' - \kappa x \cos(\phi)}{(\gamma + \gamma')^2 - \kappa^2} \qquad (57)$$

$$Re(\chi^{(1)}(\delta = 0)) = \frac{N \mu'^2}{\varepsilon_0 \hbar} \frac{-\kappa x \sin(\phi)}{(\gamma + \gamma')^2 - \kappa^2} \qquad (58)$$

$$Im(\chi^{(3)}(\delta = 0)) = \frac{2 N \mu'^4}{3 \varepsilon_0 \hbar^3} \frac{-m_1 \cos(\phi) - m_2 \cos(2\phi) - m_3}{32\gamma'(\gamma + \gamma')\left((\gamma + \gamma')^2 - \kappa^2\right)^2} \qquad (59)$$

$$Re(\chi^{(3)}(\delta = 0)) = \frac{2 N \mu'^4}{3 \varepsilon_0 \hbar^3} \frac{-m_4 \sin(\phi) - m_2 \sin(2\phi)}{32\gamma'(\gamma + \gamma')\left((\gamma + \gamma')^2 - \kappa^2\right)^2} \qquad (60)$$

where

$$m_1 = 4\gamma' x^3 \kappa(\gamma + \gamma') - 6x\kappa\gamma(\gamma + \gamma') + 2\gamma x^3 \kappa(\gamma + \gamma')$$
$$- 4\kappa^3 x - \kappa^2 x^2(\gamma + \gamma') - 7\gamma' \kappa x(\gamma + \gamma')$$
$$- 4\kappa x\gamma(\gamma + \gamma') - 2x\kappa(\gamma + \gamma')^2 - \kappa x^3(\gamma + \gamma')^2$$
$$- \gamma' \kappa x^3(\gamma + \gamma') \qquad (61)$$

**ADVANCED
SCIENCE NEWS**
www.advancedsciencenews.com

annalen
der **physik**
www.ann-phys.org

$$m_2 = 2\kappa^2 x^2 \gamma' + 2\kappa^2 x^2 (\gamma + \gamma') \tag{62}$$

$$m_3 = 2\kappa^2(\gamma + \gamma')(1 + 2x^2) + 2\gamma'\kappa^2(1 - x^2) - 2\gamma'\kappa x(\gamma + \gamma')$$
$$- \kappa x^3(\gamma + \gamma')^2 + 4\gamma'(\gamma + \gamma')^3(x^2 - 1) \tag{63}$$

$$m_4 = 3\kappa\gamma' x^3(\gamma + \gamma') + 2\gamma x^3 \kappa(\gamma + \gamma') - \kappa^2 x^2(\gamma + \gamma')$$
$$- 5\gamma' x\kappa(\gamma + \gamma') - 2x\kappa(\gamma + \gamma')^2 - \kappa x^3(\gamma + \gamma') \tag{64}$$

3. Spatially Structured Optical Effects

Up to now no assumption has been made about the spatial profile of laser fields. Now, we consider the case where the incident field possesses a nontrivial structural profile which, however, is almost unaffected by the plasmonic nanostructure (marginal reflection and absorption) as it is tuned to the resonant frequencies of the lower V-type subsystem which lie well above the surface-plasmon bands of the nanostructure in which case the nanostructure is almost transparent to the impinging structured laser field. Since, the position of the quantum system is kept fixed, that is, right opposite the center of the nanosphere, we will study the role of the position of the quantum system within the structured-field landscape, which, given the fixed position of the quantum system, is translated into the dependence of the applied structured field relative to the nanostructure.

We assume that the probe field Ω_b has an orbital angular momentum $\hbar l$ along the propagation axis z.[1,75] In this case, the vortex probe field Ω_b is characterized by the Rabi frequency

$$\Omega_b = A_b \exp(il\Phi) \tag{65}$$

For a Laguerre–Gaussian (LG) doughnut beam we may write the amplitude of a vortex beam A_b as

$$A_b(\varrho) = |\Omega_b| \left(\frac{\varrho}{w}\right)^{|l|} \exp\left(-\frac{\varrho^2}{w^2}\right) \tag{66}$$

where $\Phi = \tan^{-1}(y/x)$ is the azimuthal angle, x and y are transverse directions, $\varrho = \sqrt{x^2 + y^2}$ represents the distance from the vortex core (cylindrical radius), w denotes the beam waist parameter, and $|\Omega_b|$ is the strength of the vortex beam. The Rabi frequency of the other probe field does not have a vortex and is given by

$$\Omega_a = |\Omega_a| \tag{67}$$

In this case, Equations (19)–(31) for the evolution of the system and their corresponding coefficients remain the same, with the only difference that ϕ changes to $l\Phi$. In addition, Equations (43) and (44) will describe the azimuthally and radial varying linear and nonlinear susceptibilities, yet one needs to perform under the transformations $\phi \to l\Phi$ and $x \to X(\frac{\varrho}{w})^{|l|} \exp(-\frac{\varrho^2}{w^2})$, where $X = \frac{|\Omega_b|}{|\Omega_a|}$ in the corresponding coefficients given in Equations (45)–(56). This allows to study the spatial modification, azimuthal modulation and radial modification, of the linear and

nonlinear response of a weak non-vortex probe field Ω_a at weak intensity regime.

We will consider a situation where the laser fields are at exact resonance with the corresponding transitions ($\delta = 0$). We also assume that the quantum system is degenerate ($\omega_{32} = 0$). In this case, the imaginary part of Equation (43) for the linear absorption of probe field Ω_a simplifies to

$$Im(\chi^{(1)}(\delta = 0)) = \frac{N\mu'^2}{\varepsilon_0 \hbar} \frac{(\gamma + \gamma') - \kappa X(\frac{\varrho}{w})^{|l|} \exp(-\frac{\varrho^2}{w^2}) \cos(l\Phi)}{(\gamma + \gamma')^2 - \kappa^2} \tag{68}$$

Equation (68) implies that the linear absorption of the probe field Ω_a can be influenced by the vortex probe beam Ω_b through the term $\kappa X(\frac{\varrho}{w})^{|l|} \exp(-\frac{\varrho^2}{w^2}) \cos(l\Phi)$. This term contains a phase factor $l\Phi$ accounting for the spatial variation of the probe absorption, as well as, a radial dependence. It is indeed the existence of the quantum interference term κ, which makes the quantum system sensitive to the azimuthal phase, resulting in the spatially dependent linear absorption when the quantum system is near the plasmonic nanostructure ($d \neq 0$), as shown in **Figure 2**.

In the figures below we plot and discuss the spatial dependence of $\chi^{(1)}$ and $\chi^{(3)}$. We note that $\chi^{(1)}$ and $\chi^{(3)}$ are plotted in units of $\frac{N\mu'^2}{\varepsilon_0\hbar\Gamma_0}$ and $\frac{2N\mu'^4}{3\varepsilon_0\hbar^3\Gamma_0^3}$, respectively. In SI units, $\chi^{(1)}$ is dimensionless and $\chi^{(3)}$ has the units m²/V². The values presented here for $\chi^{(1)}$ are comparable to the values in free-space vacuum, while the values for $\chi^{(3)}$ are larger than those in free-space vacuum.

Figure 2 demonstrates the resulting absorption spectra for different values of the distance d. The results are presented in Figure 2 for two different vorticities $l = 1$ (Figure 2a–d) and $l = 2$ (Figure 2e–h). From Figure 2, we observe that the linear absorption increases with the distance d for the whole region of transverse spatial profile. The spatially structured absorption profiles oscillate sinusoidally in the presence of the plasmonic nanostructure (see also Equation (68)). We also note that there is also a radial modification with the change of l, which comes the term $(\rho/w)^{|l|}$, which is also observed in Figure 2, as well as, in the rest of the figures below.

Equation (68) implies that the linear absorption of the system for the transition $|0\rangle \leftrightarrow |2\rangle$ of the quantum system near the plasmonic nanostructure can be manipulated through the winding number l (OAM number). The l factor in the cosine term of Equation (68) governs the number of absorption peaks (or dips) in the transverse (x–y) plane. The periodic oscillatory behavior of the absorption profile in the transverse plane for a given value of distance $d = 0.4c/\omega_c$ but different OAM numbers $l = 1$ to 6 is observed in **Figure 3**. Because of the angular dependence, the spatially structured absorption profile displays a l-fold symmetry. The number of absorption peaks (or dips) increases with larger winding number l. As a result, one can easily distinguish an unknown vorticity of a vortex probe beam Ω_b solely by counting the bright spots appearing in the absorption profile of the probe field Ω_a. Furthermore, the maximum of the linear absorption curve is enhanced in some regions of the transverse plane by increasing the winding number, while gain appears in some other regions, see, for example, Figure 3f, which results from the fact that for specific azimuthal angles and radial distances $Im(\chi^{(1)}(\delta = 0))$ becomes negative. Since the denominator
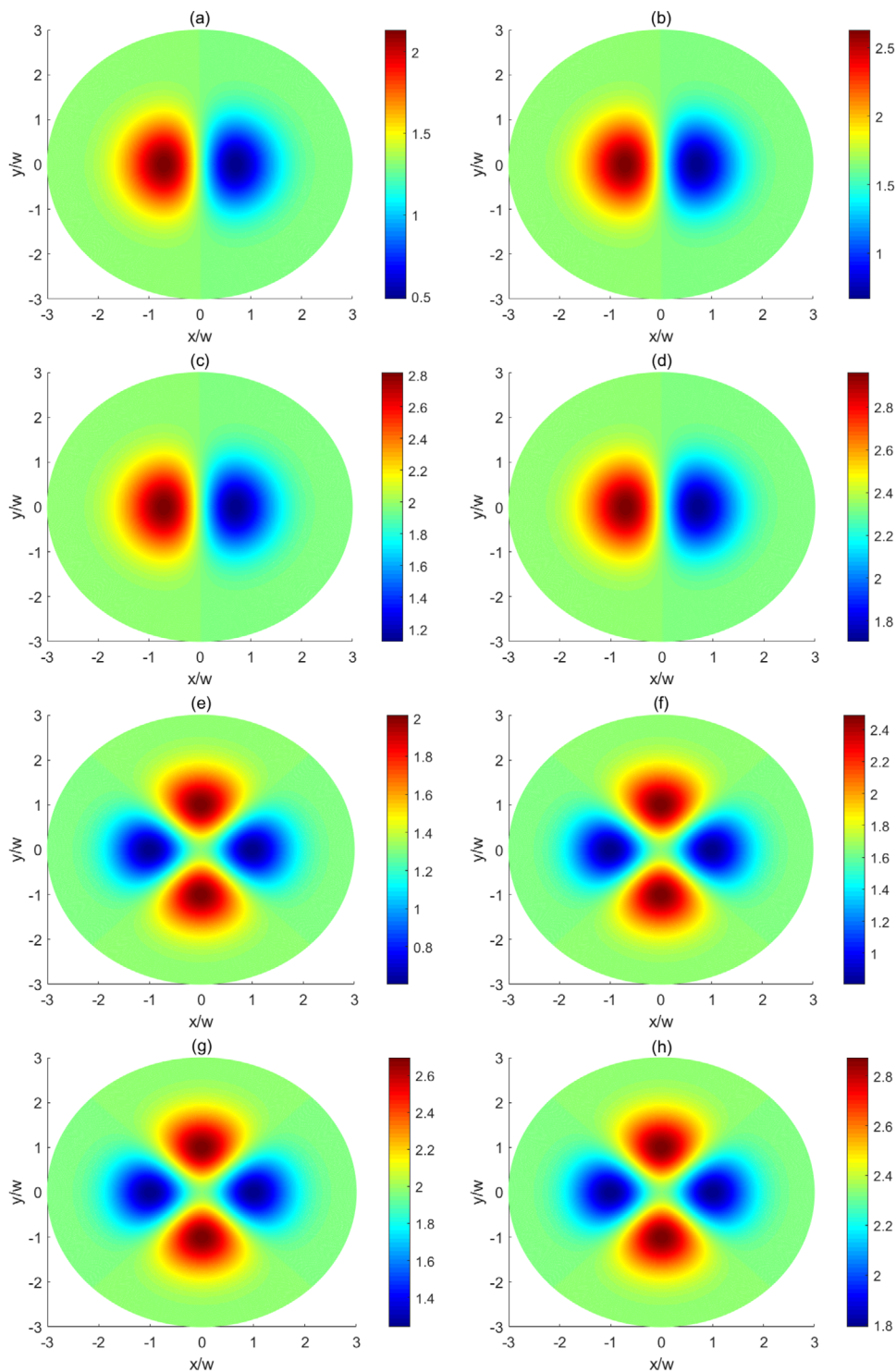
**ADVANCED
SCIENCE NEWS**

www.advancedsciencenews.com

annalen
der **physik**

www.ann-phys.org

Figure 2. Spatially structured linear absorption $Im(\chi^{(1)})$ profiles of the probe beam Ω_a in units $\frac{N\mu'^2}{\varepsilon_0\hbar\Gamma_0}$, in the presence of the plasmonic nanostructure and for different values of the distance d of the quantum system from the plasmonic nanostructure: $d = 0.1c/\omega_c$ (a,e), $d = 0.3c/\omega_p$ (b,f), $d = 0.6c/\omega_p$ (c,g) and $d = 0.8c/\omega_p$ (d,h). Here, the winding number is $l = 1$ for (a,b,c,d) and $l = 2$ (e,f,g,h), while the other parameters are $\delta = 0$, $\omega_{32} = 0$, $\frac{|\Omega_b|}{|\Omega_a|} = 1.5$, $\bar{\omega} = 0.632\omega_p$, $\gamma' = 0.3\Gamma_0$ and $\gamma'' = 0$. For $d = 0.1c/\omega_c$: $\Gamma_\perp = 35.668\Gamma_0$, $\Gamma_\parallel = 0.086\Gamma_0$; for $d = 0.3c/\omega_p$: $\Gamma_\perp = 8.080\Gamma_0$, $\Gamma_\parallel = 0.015\Gamma_0$; for $d = 0.6c/\omega_p$: $\Gamma_\perp = 1.237\Gamma_0$, $\Gamma_\parallel = 0.0044\Gamma_0$; and for $d = 0.8c/\omega_p$: $\Gamma_\perp = 0.439\Gamma_0$, $\Gamma_\parallel = 0.002\Gamma_0$.

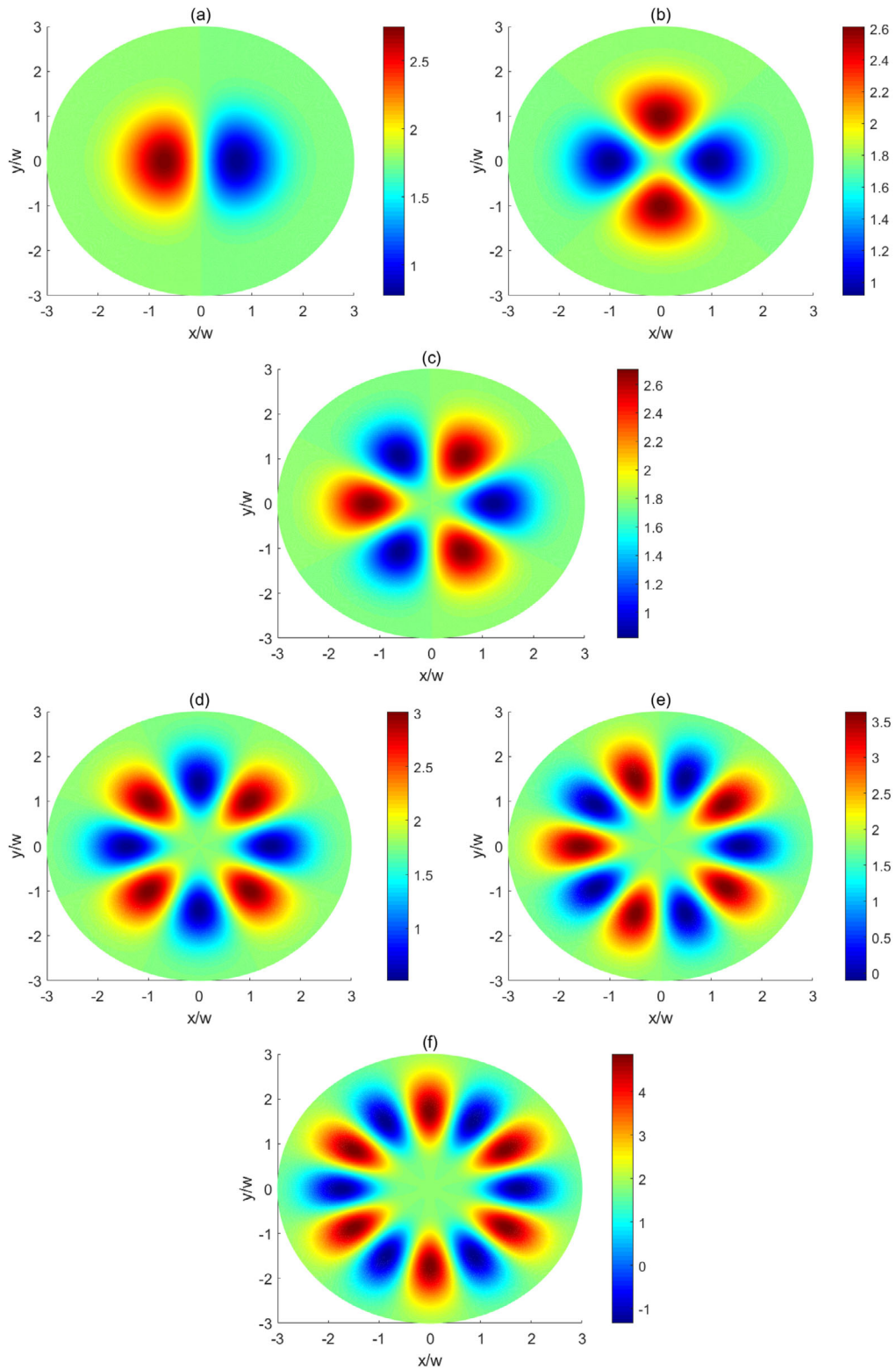**ADVANCED
SCIENCE NEWS**

www.advancedsciencenews.com

annalen
der **physik**

www.ann-phys.org

Figure 3. Spatially structured linear absorption $Im(\chi^{(1)})$ profiles of the probe beam Ω_a in units $\frac{N\mu'^2}{\varepsilon_0 \hbar \Gamma_0}$, in the presence of the plasmonic nanostructure and for different winding $l = 1$(a)$-l = 6$ (f). Here, $d = 0.4c/\omega_p$ and the other parameters are the same as Figure 2. For $d = 0.4c/\omega_c$: $\Gamma_\perp = 4.132\Gamma_0$, $\Gamma_\parallel = 0.0031\Gamma_0$.
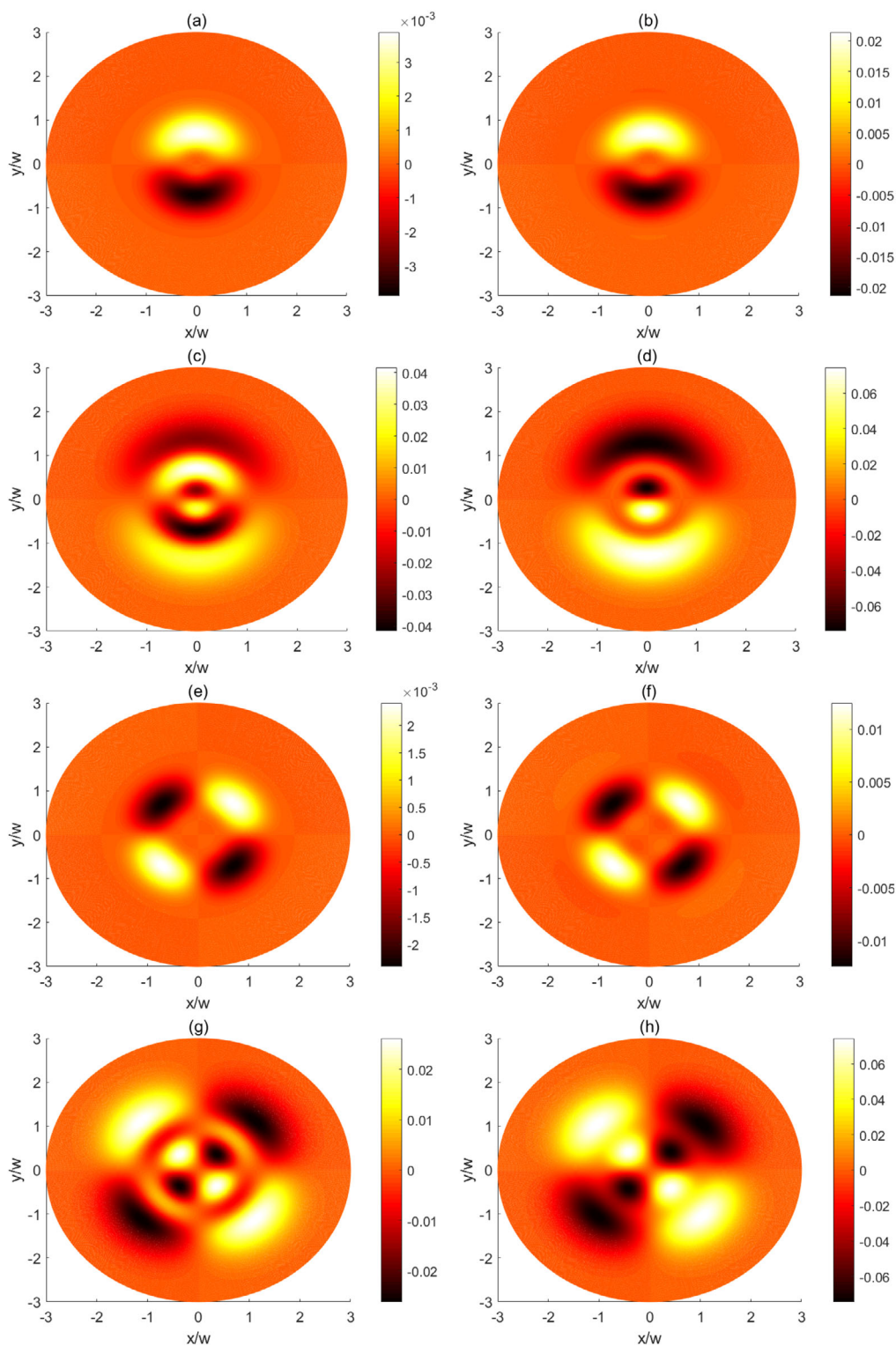
**ADVANCED
SCIENCE NEWS**

www.advancedsciencenews.com

annalen
der **physik**

www.ann-phys.org

Figure 4. Spatially structured Kerr nonlinearity $Re(\chi^{(3)})$ profiles of the probe beam Ω_a in $\frac{2N\mu'^4}{3\varepsilon_0\hbar^3\Gamma_0^3}$ units, in the presence of the plasmonic nanostructure and for different values of distance d of the quantum system from the plasmonic nanostructure: $d = 0.1c/\omega_p$ (a,e), $d = 0.3c/\omega_p$ (b,f), $d = 0.6c/\omega_p$ (c,g) and $d = 0.8c/\omega_p$ (d,h). Here, the winding number is $l = 1$ for (a,b,c,d) and $l = 2$ (e,f,g,h), and the other parameters are the same as Figure 2.
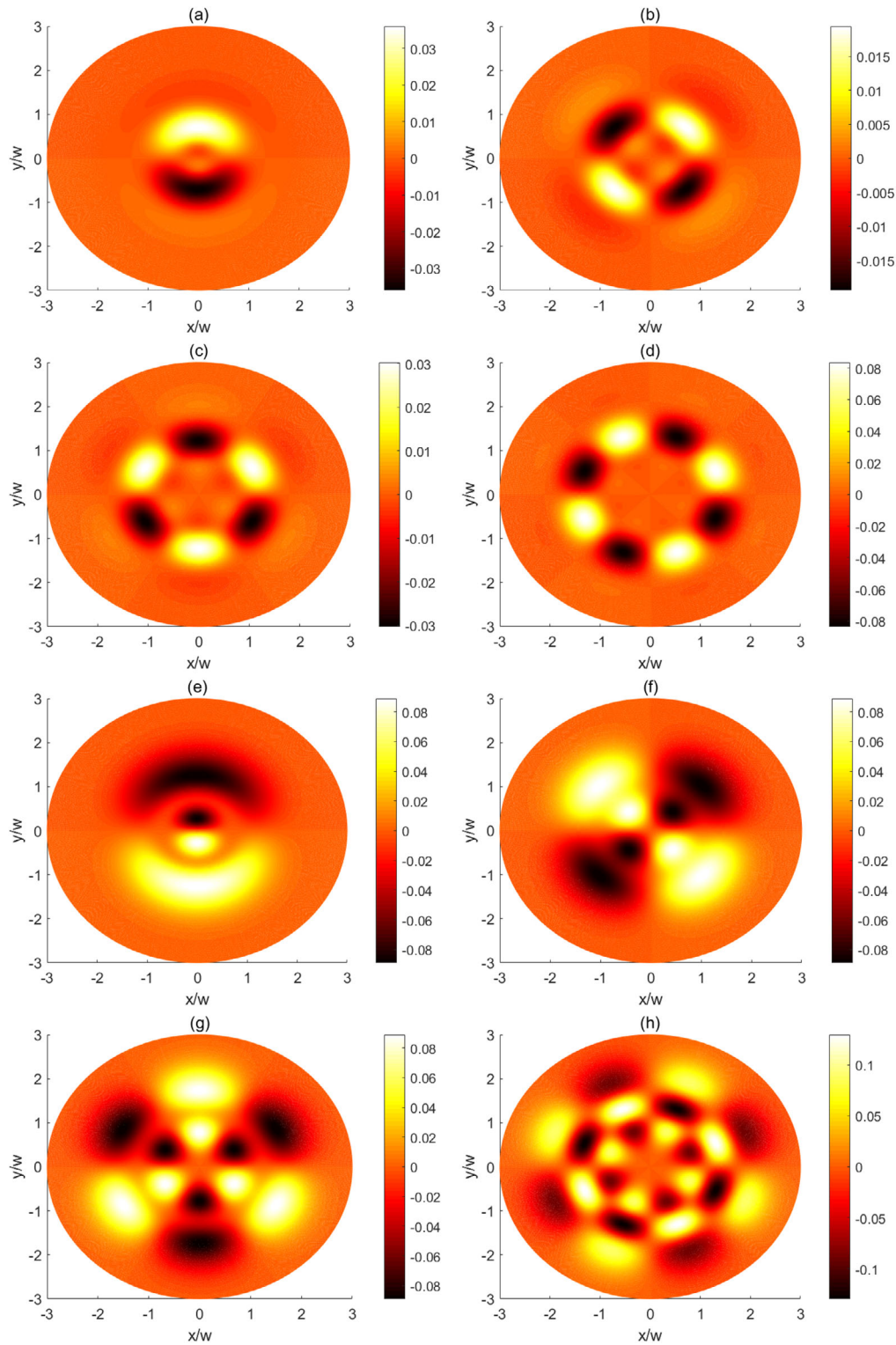
**ADVANCED
SCIENCE NEWS**

www.advancedsciencenews.com

annalen
der **physik**

www.ann-phys.org

Figure 5. Spatially structured Kerr nonlinearity $Re(\chi^{(3)})$ profiles of the probe beam Ω_a in $\frac{2N\mu'^4}{3\varepsilon_0\hbar^3\Gamma_0^3}$ units, in the presence of the plasmonic nanostructure and for different winding $l = 1$(a,e),$l = 2$ (b,f), $l = 3$ (c,g) and $l = 4$ (d,h). Here, $d = 0.4c/\omega_p$ (a,b,c,d), $d = 0.9c/\omega_p$ (e,f,g,h), and the other parameters are the same as Figure 2. For $d = 0.9c/\omega_c$: $\Gamma_\perp = 0.277\Gamma_0$, $\Gamma_\parallel = 0.0008965\Gamma_0$.

**ADVANCED
SCIENCE NEWS**

www.advancedsciencenews.com

annalen
der **physik**

www.ann-phys.org

is always positive, as $\gamma > \kappa$, the condition for the gain is $\kappa X(\frac{\varrho}{w})^{|l|} \exp(-\frac{\varrho^2}{w^2}) \cos(l\Phi) > (\gamma + \gamma')$.

In **Figures 4** and **5**, we show the Kerr nonlinearity of the medium as a function of the transverse directions x and y. As can be seen from Figure 4, the spatially-dependent Kerr nonlinearity is very sensitive to the distance from the plasmonic nanostructure. The Kerr nonlinearity is remarkably enhanced when increasing the distance parameter d. In particular, the maximal Kerr nonlinearity is enhanced by almost 10 times when we increase d from $0.1c/\omega_p$ (Figure 4a,e) to $0.3c/\omega_p$ (Figure 4b,f). Larger values of d mean higher values of the Kerr nonlinearity. However, the maximal of Kerr nonlinearity is distributed to other regions of the transverse plane (see Figure 4c–f).

Finally in Figure 5 we display how the winding number affects the Kerr nonlinearity of the system. The results show a l-fold symmetry of the Kerr nonlinearity. Moreover, very large position-dependent Kerr nonlinearities can be achieved just by increasing the winding number l.

Note that we have assumed the quantum system to be degenerated ($\omega_{32} = 0$). We have also performed calculations with non-zero ω_{32} (not shown here). We have observed a similar qualitative response for linear and nonlinear susceptibilities for $\omega_{32} \neq 0$ with that presented above with $\omega_{32} = 0$. Yet, both the linear and nonlinear susceptibilities reduce in magnitude as ω_{32} increases.

4. Conclusions

We have analyzed the light–matter interaction of a four-level double-V-type quantum system interacting with a pair of weak probe fields while located near a 2D array of metal-coated dielectric nanospheres, when one probe field carries an optical vortex, and the other field has no vortex. Because of the creation of quantum interference in spontaneous emission, the linear and nonlinear susceptibility of the non-vortex probe beam depends on the azimuthal angle and the vorticity of the twisted probe beam. This is different from an open double-V type quantum system interacting with free-space vacuum, as no quantum interference occurs in that case. Thanks to the angular dependence of the optical susceptibility for the quantum system we can obtain regions of high or low transmission as well as regions of large or small nonlinearity. We have then investigated the effect of different parameters, like the distance of the quantum system from the surface of plasmonic nanostructure and the vorticity of the twisted probe beam, and analyzed their effect on the spatial structure of the susceptibilities.

We stress that in this work we analyzed the linear and nonlinear susceptibilities of the non-vortex probe field in the presence of another, optical vortex, probe field. In essence, the optical vortex probe field plays the role of the control field, but it is a weak control field, and not the usual strong control field which is typically used in coherent light–matter interaction schemes in multilevel quantum systems. Spatial dependent linear and nonlinear optical phenomena will also occur in the case of this system interacting with a strong control optical vortex field, but this is beyond the scope of the present paper, and will be addressed in a future work. We also note that this work is interested in regular atomic densities and not large atomic densities, where dipole–dipole interactions (local field effects) need to be considered. For example,

typical atomic densities for which our work is valid are $N = 10^{20}$ m^{-3}. For large atomic densities, where dipole–dipole interactions appear to be important, one may use the Clausius–Mossotti formula for calculating the linear optical response of the system, or use proper expansions for calculating the nonlinear optical response of the system.[76] In those cases, the single quantum system result also plays an important role and therefore one expects that spatially dependent effects will also occur when the effects of dipole–dipole interactions are considered, but the actual optical response will depend on the strength of the dipole–dipole interactions. This is also beyond the scope of the present work, and we intend to study it in another future work. The results obtained here can be used in optoelectronics and quantum information processing and may find potential applications in the storage of high-dimensional optical information in phase dependent quantum memories.

Conflict of Interest

The authors declare no conflict of interest.

Data Availability Statement

Research data are not shared.

[1] J.-W. Wang, F. Castellucci, S. Franke-Arnold, *AVS Quantum Sci.* **2020**, *2*, 031702.
[2] A. Vaziri, J.-W. Pan, T. Jennewein, G. Weihs, A. Zeilinger, *Phys. Rev. Lett.* **2003**, *91*, 227902.
[3] M. Woerdemann, C. Alpmann, M. Esseling, C. Denz, *Laser Photon. Rev.* **2013**, *7*, 839.
[4] D. J. Stevenson, F. G. Moore, K. Dholakia, *J. Biomed. Opt.* **2010**, *15*, 041503.
[5] M. P. Macdonald, L. Paterson, K. V. Sepulveda, J. Arlt, W. Sibbett, K. Dholakia, *Science* **2002**, *296*, 1101.
[6] V. E. Lembessis, M. Babiker, *Phys. Rev. A* **2010**, *82*, 051402.
[7] V. E. Lembessis, D. Ellinas, M. Babiker, O. Al-Dossary, *Phys. Rev. A* **2014**, *89*, 053616.
[8] Q.-F. Chen, B.-S. Shi, Y.-S. Zhang, G.-C. Guo, *Phys. Rev. A* **2008**, *78*, 053810.
[9] G. Walker, A. S. Arnold, S. Franke-Arnold, *Phys. Rev. Lett.* **2012**, *108*, 243601.
[10] D.-S. Ding, Z.-Y. Zhou, B.-S. Shi, X.-B. Zou, G.-C. Guo, *Opt. Lett.* **2012**, *37*, 3270.
[11] L. Han, M. Cao, R. Liu, H. Liu, W. Guo, D. Wei, S. Gao, P. Zhang, H. Gao, F. Li, *Europhys. Lett.* **2012**, *99*, 34003.
[12] N. Radwell, T. W. Clark, B. Piccirillo, S. M. Barnett, S. Franke-Arnold, *Phys. Rev. Lett.* **2015**, *114*, 123603.
[13] S. Sharma, T. N. Dey, *Phys. Rev. A* **2017**, *96*, 033811.
[14] H. R. Hamedi, V. Kudriasov, J. Ruseckas, G. Juzeliunas, *Opt. Express* **2018**, *26*, 28249.

[15] S. Sharma, T. N. Dey, *J. Opt. Soc. Am. B* **2019**, *36*, 960.

[16] J. Qiu, Z.-P. Wang, B. Yu, *Quant. Inf. Process.* **2019**, *18*, 160.

[17] Rahmatullah, Muqaddar Abbas, Ziauddin, Sajid Qamar, *Phys. Rev. A* **2020**, *101*, 023821.

[18] J. Ruseckas, G. Juzeliūnas, P. Öhberg, S. M. Barnett, *Phys. Rev. A* **2007**, *76*, 053822.

[19] J. Ruseckas, A. Mekys, G. Juzeliūnas, *Phys. Rev. A* **2011**, *83*, 023812.

[20] Z. Dutton, J. Ruostekoski, *Phys. Rev. Lett.* **2004**, *93*, 193602.

[21] J. Ruseckas, V. c. v. Kudriasov, I. A. Yu, G. Juzeliūnas, *Phys. Rev. A* **2013**, *87*, 053840.

[22] D. Moretti, D. Felinto, J. W. R. Tabosa, *Phys. Rev. A* **2009**, *79*, 023825.

[23] D. Bortman-Arbiv, A. D. Wilson-Gordon, H. Friedmann, *Phys. Rev. A* **2001**, *63*, 031801.

[24] H. R. Hamedi, E. Paspalakis, G. Zlabys, G. Juzeliūnas, J. Ruseckas, *Phys. Rev. A* **2019**, *100*, 023811.

[25] J. Qiu, Z.-P. Wang, D.-S. Ding, W. Li, B. Yu, *Opt. Express* **2020**, *28*, 2975.

[26] F. Wang, F.-G. Hu, J. Xu, X.-D. Wang, *J. Opt. Soc. Am. B* **2020**, *37*, 902.

[27] Z.-P. Wang, Y.-F. Zhang, E. Paspalakis, B. Yu, *Phys. Rev. A* **2020**, *102*, 063509.

[28] J. Qiu, Z.-P. Wang, D.-S. Ding, Z.-X. Huang, B. Yu, *Phys. Rev. A* **2020**, *102*, 033516.

[29] M. Mahdavi, Z. A. Sabegh, M. Mohammadi, M. Mahmoudi, H. R. Hamedi, *Phys. Rev. A* **2020**, *101*, 063811.

[30] S. Evangelou, V. Yannopapas, E. Paspalakis, *Phys. Rev. A* **2012**, *86*, 053811.

[31] E. Paspalakis, S. Evangelou, V. Yannopapas, A. F. Terzis, *Phys. Rev. A* **2013**, *88*, 053832.

[32] L. Wang, Y. Gu, H. Chen, J.-Y. Zhang, Y. Cui, B. D. Gerardot, Q.-H. Gong, *Scient. Rep.* **2013**, *3*, 2879.

[33] S. M. Sadeghi, *Nanotechnology* **2010**, *21*, 455401.

[34] S. M. Sadeghi, *Phys. Rev. A* **2013**, *88*, 013831.

[35] D. Zhao, Y. Gu, J. Wu, J. Zhang, T. Zhang, B. D. Gerardot, Q. Gong, *Phys. Rev. B* **2014**, *89*, 245433.

[36] F. Carreño, M. A. Antón, V. Yannopapas, E. Paspalakis, *Phys. Rev. B* **2017**, *95*, 195410.

[37] V. Yannopapas, E. Paspalakis, N. V. Vitanov, *Phys. Rev. Lett.* **2009**, *103*, 063602.

[38] S. Evangelou, V. Yannopapas, E. Paspalakis, *Phys. Rev. A* **2011**, *83*, 023819.

[39] Y. Gu, L. Wang, P. Ren, J.-X. Zhang, T.-C. Zhang, J.-P. Xu, S.-Y. Zhu, Q.-H. Gong, *Plasmonics* **2012**, *7*, 33.

[40] Y. Gu, L. Wang, P. Ren, J.-X. Zhang, T.-C. Zhang, O. J. F. Martin, Q.-H. Gong, *Nano Lett.* **2012**, *12*, 2488.

[41] F. Carreño, M. A. Antón, V. Yannopapas, E. Paspalakis, *Physical Review A* **2017**, *95*, 043825.

[42] W. Zhang, A. O. Govorov, G. W. Bryant, *Phys. Rev. Lett.* **2006**, *97*, 146804.

[43] R. D. Artuso, G. W. Bryant, *Phys. Rev. B* **2010**, *82*, 195419.

[44] M. R. Singh, D. G. Schindel, A. Hatef, *Appl. Phys. Lett.* **2011**, *99*, 181106.

[45] N. Iliopoulos, A. F. Terzis, V. Yannopapas, E. Paspalakis, *Phys. Rev. B* **2017**, *96*, 075405.

[46] M. G. G. Abad, M. Mahmoudi, *Eur. Phys. J. Plus* **2020**, *135*, 352.

[47] S. H. Asadpour, M. Jafari, *Opt. Commun.* **2018**, *421*, 125.

[48] S. H. Asadpour, A. Panahpour, M. Jafari, *Eur. Phys. J. Plus* **2018**, *133*, 411.

[49] Y. You, Y.-H. Qi, Y.-P. Niu, S.-Q. Gong, *J. Phys.: Condens. Matter* **2019**, *31*, 105801.

[50] A. Vafafard, M. Sahrai, V. Siahpoush, H. R. Hamedi, S. H. Asadpour, *Sci. Rep.* **2020**, *10*, 16684.

[51] A. V. Malyshev, V. A. Malyshev, *Phys. Rev. B* **2011**, *84*, 035314.

[52] B. S. Nugroho, V. A. Malyshev, J. Knoester, *Phys. Rev. B* **2015**, *92*, 165432.

[53] M. R. Singh, *Nanotechnology* **2013**, *24*, 125701.

[54] J.-B. Li, N.-C. Kim, M.-T. Cheng, L. Zhou, Z.-H. Hao, Q.-Q. Wang, *Opt. Express* **2012**, *20*, 1856.

[55] S. K. Singh, M. K. Abak, M. E. Tasgin, *Phys. Rev. B* **2016**, *93*, 035410.

[56] S. Evangelou, V. Yannopapas, E. Paspalakis, *J. Mod. Opt.* **2014**, *61*, 1458.

[57] H. Chen, J. Ren, Y. Gu, D.-X. Zhao, J. Zhang, Q. Gong, *Sci. Rep.* **2016**, *5*, 18315.

[58] A. F. Terzis, S. G. Kosionis, J. Boviatsis, E. Paspalakis, *J. Mod. Opt.* **2016**, *63*, 451.

[59] J. Ren, H. Chen, Y. Gu, D.-X. Zhao, H. Zhou, J. Zhang, Q. Gong, *Nanotechnology* **2016**, *27*, 425205.

[60] M. M. Tohari, A. Lyras, M. S. AlSalhi, *Nanomaterials* **2018**, *8*, 521.

[61] S. G. Kosionis, E. Paspalakis, *J. Phys. Chem. C* **2019**, *123*, 7308.

[62] X.-N. Liu, N. Kongsuwan, X.-G. Li, D.-X. Zhao, Z.-M. Wu, O. Hess, X.-H. Zhang, *J. Phys. Chem. Lett.* **2019**, *10*, 7594.

[63] H. R. Hamedi, V. Yannopapas, A. Mekys, E. Paspalakis, *Phys. E* **2021**, *110*, 114662.

[64] G. S. Agarwal, *Phys. Rev. Lett.* **2000**, *84*, 5500.

[65] M. Kiffner, M. Macovei, J. Evers, C. H. Keitel, *Prog. Opt.* **2010**, *55*, 85.

[66] Y. Yang, J. Xu, H. Chen, S. Zhu, *Phys. Rev. Lett.* **2008**, *100*, 043601.

[67] G.-X. Li, J. Evers, C. H. Keitel, *Phys. Rev. B* **2009**, *80*, 045102.

[68] P. K. Jha, X. Ni, C. Wu, Y. Wang, X. Zhang, *Phys. Rev. Lett.* **2015**, *115*, 025501.

[69] S. Hughes, G. S. Agarwal, *Phys. Rev. Lett.* **2017**, *118*, 063601.

[70] V. Karanikolas, E. Paspalakis, *J. Phys. Chem. C* **2018**, *122*, 14788.

[71] N. Stefanou, V. Yannopapas, A. Modinos, *Comp. Phys. Commun.* **1998**, *113*, 49.

[72] N. Stefanou, V. Yannopapas, A. Modinos, *Comp. Phys. Commun.* **2000**, *132*, 189.

[73] R. Sainidou, N. Stefanou, A. Modinos, *Phys. Rev. B* **2004**, *69*, 064301.

[74] D. Bortman-Arbiv, A. D. Wilson-Gordon, H. Friedmann, *Phys. Rev. A* **2001**, *63*, 043818.

[75] L. Allen, M. J. Padgett, M. Babiker, *Prog. Opt.* **1999**, *39*, 291.

[76] K. Dolgaleva, R. W. Boyd, *Adv. Opt. Photon.* **2012**, *4*, 1.